Inorg. Chem. **2007**, *46*, 7509–7521

Lead-Poisoned Zinc Fingers: Quantum Mechanical Exploration of Structure, Coordination, and Electronic Excitations

Andrzej A. Jarzęcki*

Department of Chemistry, Graduate Center, and Brooklyn College, the City University of New York, Brooklyn, New York 11210

Received April 17, 2007

Density functional theory (DFT) structure calculations and time-dependent DFT electronic excitation calculations on simple mononuclear lead structures confirm recent reports on the stabilization of tricoordinated structural domains in poisoned proteins. However, the possibility of the formation of tetracoordinated lead complexes should not be disregarded in studies on mechanisms of lead toxicity because structures with both coordination modes are plausible and might contribute to observed UV spectra. Reported calculations along with detailed molecular orbital analysis confirm that the intense UV signal at around 260 nm is an indicator of the ligand-to-metal charge transfer (LMCT) band where the electrons are transferred from the sulfur 3p orbital to the lead 6p orbital. The composition of the LMCT band reveals significant excitations not only from the Pb–S bonding orbitals but also from sulfur lone-pair orbitals to the Pb–S antibonding orbitals for which the electron density is largely localized on the Pb "6p-like" molecular orbitals. There is a solid indication that the stereochemically active pair orbital of lead is not strongly hybridized and remains largely of the 6s character in tricoordinated lead structures and is minimally hybridized in tetracoordinated lead structures. Computed UV spectra of lead model complexes are compared to experimental UV spectra of model lead peptides. The comparison shows a good agreement with the major spectral trends and changes observed in these experiments.

Introduction

Lead poisoning is an environmental disease. Exposure to the metal may occur from contact with lead-contaminated dust, water, food, and soil. Lead production and its environmental contamination dramatically increased during the Roman Empire when lead was extensively used for manufacturing drinking vessels, water pipes, and coins and was even intentionally added to wine to conserve its sweetness.[1−3] In modern times, lead has been used extensively in paints, cosmetics, batteries, pipes, solder, and ammunition.[4] The poison is cumulative and the toxic effects are severe, but increasing knowledge on lead toxicity has been our best prevention against its adverse health effects. This is clearly demonstrated by the fact that the "safe" threshold for the blood lead level (BLL) has been revised downward 6-fold during the past 30 years, from 60 μg/dL prior to 1971, 40 μg/dL until 1978, 30 μg/dL until 1985, and 25 μg/dL from 1985 until 1991, when the threshold was changed to the present <10 μg/dL level.[5−8] This progressive reduction over time in the toxic threshold of lead (a similar trend seen with most other chemicals) results from an accumulation of data, more sophisticated tools and methodology to measure adverse toxic effects, and an improved understanding of lead's cellular targets. As a result, the prohibition of many lead products in the United States—especially of leaded gasoline, residential lead paint, and lead from solder in canned food containers—has drastically reduced the average BLL of U.S.

* To whom correspondence should be addressed: E-mail: jarzecki@brooklyn.cuny.edu. Tel.: 1-718-951-5000, ext. 2822.

(1) Nriagu, J. O. *Lead and Lead Poisoning in Antiquity*; John Wiley & Sons, Inc.: New York, 1986.
(2) Nriagu, J. O. *N. Engl. J. Med.* **1983**, *308*, 660−663.
(3) Hong, S.; Candelone, J.-P.; Patterson, C. C.; Boutron, C. F. *Science* **1994**, *265*, 1841−1843.
(4) Christensen, J. M.; Kristiansen, J. In *Handbook on Metals in Clinical and Analytical Chemistry*; Seiler, H. G., Sigel, A., Sigel, H., Eds.; Marcel Dekker: New York, 1994; pp 425−440.
(5) *Increased Lead Absorption and Lead Poisoning in Young Children*; Centers for Disease Control and Prevention: Atlanta, GA, 1975.
(6) *Preventing Lead Poisoning in Young Children*; Centers for Disease Control and Prevention: Atlanta, GA, 1978.
(7) *Second Revision of the Statement on Preventing Lead Poisoning in Young Children*; Centers for Disease Control and Prevention: Atlanta, GA, 1985.
(8) *Fourth Revision of the Statement on Preventing Lead Poisoning in Young Children*; Centers for Disease Control and Prevention: Atlanta, GA, 1991.

10.1021/ic700731d CCC: $37.00
Published on Web 08/04/2007

children since 1978.[8] However, the most recent Centers for Disease Control and Prevention estimates state that 310 000 children under 6 years of age still have a BLL above the present safe threshold and approximately 24 million housing units in the United States have deteriorated leaded paint and elevated levels of lead-contaminated household dust.[9] Furthermore, recent developments on neurotoxicity report that lead can impair a child's development even at BLLs below the safe 10 μg/dL level. In the release of the comprehensive "Third National Report on Exposure to Chemicals in Humans", it was unequivocally stated that a safe BLL in children simply does not exist,[10] and the U.S. Department of Health and Human Services has established an ambitious goal of eliminating elevated BLLs in children by 2010.[9]

It is known that lead toxicity comes from its ability to mimic other biologically important metals, the most notable of which are calcium[11,12] and zinc.[12−14] Detailed biophysical studies have revealed that lead binds to thiolate-rich structural zinc sites many orders of magnitude more tightly than to calcium ones[15,16] and that when lead binds to zinc-binding proteins, it poisons the protein by inducing new coordination and structural preferences.[16−18] These fundamental molecular changes bring different functions, and as a result, the poisoned protein fails to catalyze particular enzymatic reactions or to carry out its identifiable purposes.[19−23]

Probing zinc-binding domains with electronic spectroscopy poses an experimental challenge. The zinc is spectroscopically silent due to its inert d^{10} electronic configuration, excluding d−d transitions and deficiency in intra-atomic or applicable charge-transfer (CT) transitions. Unlike zinc, lead, despite its d^{10} configuration, is *not* spectroscopically silent. Lead bound to cysteine residues in proteins results in the appearance of several intense absorption bands in the ultraviolet (UV) region.[15,17,24] These absorption bands have been used to monitor the stability of lead−protein interactions,[15−18,24−28] but there has not yet been a detailed study of the electronic origin of these bands and their relation to lead coordination and structure. The photoelectron spectroscopy suggests that the most likely assignment for the CT transitions observed for lead−thiolate compounds is S(3p) → Pb(6p) ligand-to-metal charge transfer (LMCT),[16,29] possibly with some mixing of Pb(6s) character into the Pb(6p) orbitals.[30] However, detailed experimental and theoretical studies on lead−thiolate photoelectron and absorption spectroscopy have not yet been undertaken. Furthermore, the Pb-Cys CT transitions are of fundamental interest since they are essential for distinguishing Pb−S vibrational frequency modes against the background of the protein frequency modes in resonance Raman enhancement experiments. Analogous to those of Pb−S, the Cd−S and Hg−S CT bands have been already applied to monitor cysteine and histidine ligands in cadmium-[31] and mercury-substituted[32] zinc-binding peptides via UV resonance Raman spectroscopy. This spectroscopy, combined with computational modeling, gives a feasible opportunity to reveal various lead-binding domains and to investigate the biochemical mechanisms of lead poisoning.

Lead structural chemistry has received relatively little attention when compared with the chemistry of transition metals. However, pioneering structural studies by Payne, Raymond, and others have revealed that Pb(II) exhibits a rich and interesting coordination chemistry.[33−47] Most com-

(9) *Fifth Revision of the Statement on Preventing Lead Poisoning in Young Children*; Centers for Disease Control and Prevention: Atlanta, GA, 2005.
(10) *Third National Report on Human Exposure to Environmental Chemicals*; Centers for Disease Control and Prevention: Atlanta, GA, 2005. http://www.cdc.gov/exposurereport/3rd/pdf/thirdreport.pdf.
(11) Simons, T. J. B. *Neurotoxicology* **1993**, *14*, 77−86.
(12) Garza, A.; Vega, R.; Soto, E. *Med. Sci. Monit.* **2006**, *12*, RA57−65.
(13) Simons, T. J. B. *Eur. J. Biochem.* **1995**, *234*, 178−183.
(14) Zawia, N. H.; Crumpton, T.; Brydie, M.; Reddy, G. R.; Razmiafshari, M. *Neurotoxicology* **2000**, *21*, 1069−1080.
(15) Godwin, H. A. *Curr. Opin. Chem. Biol.* **2001**, *5*, 223−227.
(16) Claudio, E. S.; Godwin, H. A.; Magyar, J. S. *Prog. Inorg. Chem.* **2003**, *51*, 1−144.
(17) Payne, J. C.; ter Horst, M. A.; Godwin, H. A. *J. Am. Chem. Soc.* **1999**, *121*, 6850−6855.
(18) Magyar, J. S.; Weng, T.-C.; Stern, C. M.; Dye, D. F.; Rous, B. W.; Payne, J. C.; Bridgewater, B. M.; Mijovilovich, A.; Parkin, G.; Zaleski, J. M.; Penner-Hahn, J. E.; Godwin, H. A. *J. Am. Chem. Soc.* **2005**, *127*, 9495−9505.
(19) Hanas, J. S.; Rodgers, J. S.; Bantle, J. A.; Chang, Y.-G. *Mol. Pharmacol.* **1999**, *56*, 982−988.
(20) Quintanilla-Vega, B.; Hoover, D. J.; Bal, W.; Silbergeld, E. K.; Waalkes, M. P.; Anderson, L. D. *Chem. Res. Toxicol.* **2000**, *13*, 594−600.
(21) Razmiafshari, M.; Kao, J.; d'Avignon, A.; Zawia, N. H. *Toxicol. Appl. Pharmacol.* **2001**, *172*, 1−10.
(22) Jaffe, E. K.; Martins, J.; Li, J.; Kervinen, J.; Dunbrack, L., Jr. *J. Biol. Chem.* **2001**, *276*, 1531−1537.
(23) Huang, M.; Krepkiy, D.; Hu, W.; Petering, D. H. *J. Inorg. Biochem.* **2004**, *98*, 775−785.
(24) Busenlehner, L. S.; Cosper, N. J.; Scott, R. A.; Rosen, B. P.; Wong, M. D.; Giedroc, D. P. *Biochemistry* **2001**, *40*, 4426−4436.
(25) Cheng, Y.; Yan, Y.-B.; Liu, J. *J. Inorg. Biochem.* **2005**, *99*, 1952−1962.
(26) Ghering, A. B.; Miller Jenkins, L. M.; Schenck, B. L.; Deo, S.; Mayer, R. A.; Pikaart, M. J.; Omichinski, J. G.; Godwin, H. A. *J. Am. Chem. Soc.* **2005**, *127*, 3751−3759.
(27) Ghering, A. B.; Shokes, J. E.; Scoot, R. A.; Omichinski, J. G.; Godwin, H. A. *Biochemistry* **2004**, *43*, 8346−8355.
(28) Matzapetakis, M.; Ghosh, D.; Weng, T.-C.; Penner-Hahn, J. E.; Pecoraro, V. L. *J. Biol. Inorg. Chem.* **2006**, *11*, 876−890.
(29) Vogler, A.; Nikol, H. *Pure Appl. Chem.* **1992**, *64*, 1311−1317.
(30) McFeely, F. R.; Kowalczyk, S.; Ley, L.; Pollak, R. A.; Shirley, D. A. *Phys. Rev. B: Solid State* **1973**, *7*, 5228−5237.
(31) Vargek, M.; Zhao, X.; Lai, Z.; McLendon, G. L.; Spiro, T. G. *Inorg. Chem.* **1999**, *38*, 1372−1373.
(32) Fleissner, G.; Kozlowski, P. M.; Vargek, M.; Bryson, J. W.; O'Halloran, T. V.; Spiro, T. G. *Inorg. Chem.* **1999**, *38*, 3523−3528.
(33) Dean, P. A. W.; Vittal, J. J.; Payne, N. C. *Inorg. Chem.* **1984**, *23*, 4232−4236.
(34) Dean, P. A. W.; Vittal, J. J.; Payne, J. C. *Inorg. Chem.* **1985**, *24*, 3594−3997.
(35) Abu-Dari, K.; Hahn, F. E.; Raymond, K. N. *J. Am. Chem. Soc.* **1990**, *112*, 1519−1524.
(36) Reger, D. L.; Huff, M. F.; Rheingold, A. L.; Haggerty, B. S. *J. Am. Chem. Soc.* **1992**, *114*, 579−584.
(37) Abu-Dari, K.; Karpishin, T. B.; Raymond, K. N. *Inorg. Chem.* **1993**, *32*, 3052−3055.
(38) Bashall, A.; McPartlin, M.; Murphy, B. P.; Powell, H. R.; Waikar, S. *J. Chem. Soc., Dalton Trans.* **1994**, 1383−1994.
(39) Rupprecht, S.; Franklin, S. J.; Raymond, K. N. *Inorg. Chim. Acta* **1995**, *235*, 185−195.
(40) Rupprecht, S.; Langemann, K.; Lugger, T.; McCormick, J. M.; Raymond, K. N. *Inorg. Chim. Acta* **1996**, *243*, 79−90.
(41) Bridgewater, B. M.; Parkin, G. *J. Am. Chem. Soc.* **2000**, *122*, 7140−7141.
(42) Harrowfield, J. M.; Maghaminia, S.; Soudi, A. A. *Inorg. Chem.* **2004**, *43*, 1810−1812.
(43) Alvarado, R. J.; Rosenberg, J. M.; Andreu, A.; Bryan, J. C.; Chen, W.-Z.; Ren, T.; Kavallieratos, K. *Inorg. Chem.* **2005**, *44*, 7951−7959.
(44) Pedrido, R.; Bermejo, M. R.; Romero, M. J.; Vazquez, M.; Gonzalez-Noya, A. N.; Maneiro, M.; Rodriguez, M. J.; Fernandez, M. I. *Dalton Trans.* **2005**, 572−579.

mon ligands of lead have O, N, S, and P donor atoms or some combination thereof, which demonstrate a broad range of coordination numbers, varying from 2 to 12.[48−50] Lead coordination compounds are generally categorized as homodirected (symmetrical) or hemidirected (asymmetrical), which are distinguished by the disposition of ligands around the metal ion. Complexes with high coordination numbers (more than 8) usually adopt a homodirected geometry, whereas complexes with low coordination numbers (less than 6) are normally hemidirected, a ligand displacement which is commonly linked to increased effects of the chemically inert but sterochemically active $6s^2$ lone-pair orbital of lead.

In proteins, zinc adopts symmetrical tetracoordinated (tetrahedral) structural domains, and tetracoordinated lead structures in poisoned proteins were originally suggested with hemidirected structure,[16] which has an irregular tetrahedral geometry. This arrangement of ligands is derived from a trigonal-bipyramidal structure where a stereochemically active $6s^2$ lone pair occupies one of the equatorial corners just as predicted by the valence shell electron pair repulsion (VSEPR) model.[51] However, the most recent reexamination of lead(II) coordination preferences in sulfur-rich sites, applying X-ray absorption spectroscopy for Pb−peptide complexes and a few coordination compounds,[18,45] has challenged the previously suggested tetracoordination of lead and has concluded that a tricoordination mode of lead is preferred in poisoned proteins. Nevertheless, despite these significant advances, much remains unknown about typical structures, coordination, and spectroscopic properties of lead in poisoned protein.

It is only in the past decade that quantum mechanical studies began to investigate the structural chemistry of lead and the effects of its stereochemically active lone pair in both coordination compounds[52−72] and solid-state materials.[73−75] This seemingly tardy theoretical attention arose from the computational challenges associated with a comprehensive description of the heavy metals, such as lead, in quantum mechanical calculations. These obstacles were overcome with recent advances in the accuracy and reliability of relativistic effective-core potentials, density functional methods, and modern computer architecture. In the past few years, these combined advances have resulted in a noticeably increased number of computational investigations[59−72,75] relevant to lead chemistry.

The present computational study considers mononuclear lead(II) model complexes with tri- and tetracoordination modes and their predicted UV spectra. The models represent all combinations of thiolate and imidazole ligands that mimic the coordination of cysteine and histidine side chains to the metal. Hence, the computed structures might signify structural lead domains, which are responsible for the interruption and inhibition of processes facilitated by the typical structural zinc-finger domains.

The presentation is organized as follows: first, the computed structures, their coordination modes, and an influence of the stereochemically active lone pair of lead are discussed. Computed molecular geometries are compared with a set of X-ray crystal structures[33,34,36,41,45,59] and extended X-ray emission fine structure (EXEFS) spectra measurements.[18] These experimental data represent archetypes of the specific coordination modes and ligands corresponding to appropriate coordination numbers for mononuclear lead with various sulfur and nitrogen donor atoms only. We have also singled out five energetically relevant model complexes based on their estimated stability in an aqueous solution. For these representative models, we present a comprehensive analysis of molecular orbitals and connect it to the spectroscopic properties and electronic excitations for all tri- and tetracoordinated models. Finally, the computed UV spectra of model complexes are directly compared with the experimental UV spectra of model lead peptides. Observed spectral trends are discussed as a function of structure and coordination with fresh perspectives and intuitive relations of structural and spectroscopic properties for the mononuclear structural lead-binding domains.

(45) Andersen, R. J.; diTargiani, R. C.; Hancock, R. D.; Stern, C. L.; Goldberg, D. P.; Godwin, H. A. *Inorg. Chem.* **2006**, *45*, 6574−6576.
(46) Fan, S.-R.; Zhu, L.-G. *Inorg. Chem.* **2006**, *45*, 7935−7942.
(47) Xiao, H.-P.; Morsali, A. *Solid State Sci.* **2007**, *9*, 155−158.
(48) Hancock, R. D.; Martell, A. E. *Chem. Rev.* **1989**, *89*, 1875−1914.
(49) Parr, J. *Polyhedron* **1997**, *16*, 551−566.
(50) Davidovich, R. L. *Russ. J. Coord. Chem.* **2005**, *31*, 455−466.
(51) Gillespie, R. J.; Nyholm, R. S. *Q. Rev. Chem. Soc.* **1957**, *11*, 339−380.
(52) Kapp, J.; Remko, M.; Schleyer, P. v. R. *Inorg. Chem.* **1997**, *36*, 4241−4246.
(53) Shimoni-Livny, L.; Glusker, J. P.; Bock, C. W. *Inorg. Chem.* **1998**, *37*, 1853−1867.
(54) Borrmann, H.; Campbell, J.; Dixon, D. A.; Mercier, H. P. A.; Pirani, A. M.; Schrobilgen, G. J. *Inorg. Chem.* **1998**, *37*, 6656−6674.
(55) Rodriguez-Fortea, A.; Alemany, P.; Ziegler, T. *J. Phys. Chem. A* **1999**, *103*, 8288−8294.
(56) Constantine, S. P.; Cox, H.; Hitchcock, P. B.; Lawless, G. A. *Organometallics* **2000**, *19*, 317−326.
(57) Lie, W.; Fedorov, D. G.; Hirao, K. *J. Phys. Chem. A* **2002**, *106*, 7057−7061.
(58) Sigal, N.; Apeloig, Y. *Organometallics* **2002**, *21*, 5486−5493.
(59) Fleischer, H.; Schollmeyer, D. *Inorg. Chem.* **2004**, *43*, 5529−5536.
(60) Benjelloun, A. T.; Daoudi, A.; Chermette, H. *Mol. Phys.* **2005**, *103*, 317−335.
(61) Boilet, L.; Cornard, J. P.; Lapouge, C. *J. Phys. Chem. A* **2005**, *109*, 1952−1960.
(62) Cornard, J. P.; Dangleterre, L.; Lapouge, C. *J. Phys. Chem. A* **2005**, *109*, 10044−10051.
(63) Lapouge, C.; Cornard, J. P. *J. Phys. Chem. A* **2005**, *109*, 6752−6761.
(64) Lein, M.; Krapp, A.; Frenking, G. *J. Am. Chem. Soc.* **2005**, *127*, 6290−6299.
(65) Platas-Iglesias, C.; Esteban-Gomez, D.; Enriquez-Perez, T.; Avecilla, F.; de Blas, A.; Rodriguez-Blas, T. *Inorg. Chem.* **2005**, *44*, 2224−2233.
(66) Wang, X.; Andrews, L. *J. Phys. Chem. A* **2005**, *109*, 9013−9020.
(67) Zeng, H.; Schelly, Z. A.; Ueno-Noto, K.; Marynick, D. S. *J. Phys. Chem. A* **2005**, *109*, 1616−1620.
(68) Zhang, Y.; Zhang, X.; Liu, Z.; Bian, Y.; Jiang, J. *J. Phys. Chem. A* **2005**, *109*, 6363−6370.
(69) Esteban-Gomez, D.; Platas-Iglesias, C.; Enriquez-Perez, T.; Avecilla, F.; de Blas, A.; Rodriguez-Blas, T. *Inorg. Chem.* **2006**, *45*, 5407−5416.
(70) Gutle, C.; Salpin, J.-Y.; Cartailler, T.; Tortajada, J.; Gaigeot, M.-P. *J. Phys. Chem. A* **2006**, *110*, 11684−11694.
(71) Liu, H.; Xing, X.; Sun, S.; Gao, Z.; Tang, Z. *J. Phys. Chem. A* **2006**, *110*, 8688−8694.
(72) Stoltzfus, M. W.; Woodward, P. M.; Seshadri, R.; Klepeis, J.-H.; Bursten, B. *Inorg. Chem.* **2007**, *46*, 3839−3850.
(73) Terpstra, H. J.; de Groot, R. A.; Haas, C. *Phys. Rev. B: Condens. Matter Mater. Phys.* **1995**, *52*, 690−697.
(74) Watson, G. W.; Parker, S. C. *J. Phys. Chem. B* **1999**, *103*, 1258−1262.
(75) Wei, C. M.; Cheng, C.; Chang, C. M. *J. Phys. Chem. B* **2006**, *110*, 24642−24645.

Computational Details

All calculations reported here were carried out by the *Gaussian 03* program package.[76] All molecular structures are found by geometry optimization at the B3LYP/6-31G* level of density functional theory (DFT) in combination with a cc-pVDZ-PP relativistic effective-core potential[77] for lead to describe its core electrons with the [4s3p2d] composition of valence orbitals ($5s^2$-$5p^6 5d^{10} 6s^2$, i.e., 20 electrons for Pb^{2+} ion) treated explicitly in electronic structure calculations. Computed frequencies of all structures are positive, indicating that the structures are at real minima of their ground-state potential-energy surfaces, though the issue of whether the optimized minima are global was not explored. The computed binding energies of optimized structures were estimated in an aqueous solution based on single-point computed solvation energies employing the polarizable continuum model (PCM)[78] and inclusion of the zero-point energy correction.

In general, evaluation of the full potential defined by DFT (i.e., efficient inclusion of the terms of exchange and correlation potentials) cannot be done analytically and requires a numerical integration. The accuracy of this integration is achieved by employing grid points in space around the nucleus. The distribution of points and definition of the grid can be uniform (unpruned), with the same number of angular points at each radial distance, or pruned to reduce the number of points. The pruned grid uses fewer points for the shells near the core and far from the nucleus, where less density is needed for a given level of computational accuracy.[79] To achieve reliable computational accuracy for our study, we have employed the pruned 99 point Euler−Maclaurin radial grid with a 590 point angular grid for all atoms but lead. For lead atoms, we used a default unpruned grid, as implemented in the program package.

The electronic excitations in the UV spectral region were computed for structures at their minima, employing time-dependent density functional theory (TDDFT) approximation[80] at the same level of theory as that of the ground-state calculations. The ultraviolet excitations, which span the spectral region of interest, have been covered by computing the 50 lowest excited states for all structures. In addition to lead structures, corresponding zinc complexes representing healthy zinc-finger domains were computed at the same level of theory, and their predicted spectra of electronic excitations were compared with lead-poisoned structures just for the reference. All zinc structures were at their true minima and showed the expected tetrahedral coordination; however, a detailed report on zinc structures and spectroscopy is not discussed in this study.

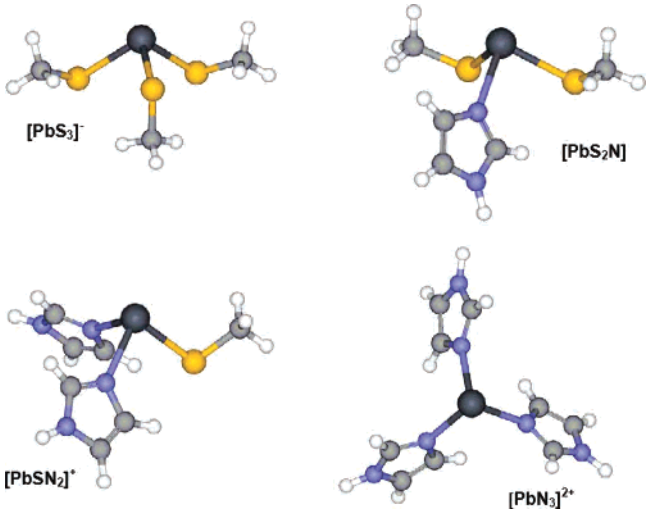

Figure 1. Molecular structures of tricoordinated lead complexes in this study.

The molecular orbital and electronic structure analysis were performed by natural population analysis as implemented in the *NBO 5.0* program package.[81] Line shapes of computed UV spectra were simulated based on computed oscillator strengths and adoption of the Lorentzian distribution with the 10 nm half-bandwidth for each computed singlet−singlet excitation.

Results and Discussion

Coordination Modes and the Lone-Pair Orbital. Computed tricoordinated lead complexes with various combinations of thiolate and histidine ligands are shown in Figure 1. All structures have a trigonal-pyramidal arrangement of ligands, as expected from the simple VSEPR model[51] for three ligands (X) of coordinated lead and one valence pair of electrons from the $6s^2$ stereochemically active lone-pair orbital (E) in a tetrahedral configuration AX_3E. Furthermore, a simple assumption in the VSEPR about the strength of electrostatic repulsion, which decreases in the order lone-pair−lone-pair > lone-pair−bond-pair > bond-pair−bond-pair, predicts that the bond angles of tricoordinated lead should be smaller than a tetrahedral angle (109°28′) due to strong lone-pair−bond-pair repulsion. As an additional justification for the observed ligand arrangement, a sp^3 hybridization of lead valence orbitals is often assigned to the tricoordination mode of lead.

Similarly, computed tetracoordinated lead structures with various combinations of thiolate and histidine ligands are shown in Figure 2. As expected from the VSERP model, four coordinated ligands and one lone pair ($6s^2$) of lead should have a ligand arrangement derived from the trigonal-bipyramidal basic shape AX_4E, where the lone pair occupies one of the vertices. Computed structures show two types of ligand arrangement: A mode A for $[PbS_4]^{2-}$ and $[PbS_3N]^-$ complexes that are characterized by one strongly bound axial ligand and three weakly bound equatorial ligands and a mode

(76) Frisch, M. J.; Trucks, G. W.; Schlegel, H. B.; Scuseria, G. E.; Robb, M. A.; Cheeseman, J. R.; Montgomery, J. J. A.; Vreven, T.; Kudin, K. N.; Burant, J. C.; Millam, J. M.; Iyengar, S. S.; Tomasi, J.; Barone, V.; Mennucci, B.; Cossi, M.; Scalmani, G.; Rega, N.; Petersson, G. A.; Nakatsuji, H.; Hada, M.; Ehara, M.; Toyota, K.; Fukuda, R.; Hasegawa, J.; Ishida, M.; Nakajima, T.; Honda, Y.; Kitao, O.; Nakai, H.; Klene, M.; Li, X.; Knox, J. E.; Hratchian, H. P.; Cross, J. B.; Bakken, V.; Adamo, C.; Jaramillo, J.; Gomperts, R.; Stratmann, R. E.; Yazyev, O.; Austin, A. J.; Cammi, R.; Pomelli, C.; Ochterski, J. W.; Ayala, P. Y.; Morokuma, K.; Voth, G. A.; Salvador, P.; Dannenberg, J. J.; Zakrzewski, V. G.; Dapprich, S.; Daniels, A. D.; Strain, M. C.; Farkas, O.; Malick, D. K.; Rabuck, A. D.; Raghavachari, K.; Foresman, J. B.; Ortiz, J. V.; Cui, Q.; Baboul, A. G.; Clifford, S.; Cioslowski, J.; Stefanov, B. B.; Liu, G.; Liashenko, A.; Piskorz, P.; Komaromi, I.; Martin, R. L.; Fox, D. J.; Keith, T.; Al-Laham, M. A.; Peng, C. Y.; Nanayakkara, A.; Challacombe, M.; Gill, P. M. W.; Johnson, B.; Chen, W.; Wong, M. W.; Gonzalez, C.; Pople, J. A. *Gaussian 03*, revision C.02; Gaussian, Inc.: Wallingford, CT, 2004.
(77) Peterson, K. A. *J. Chem. Phys.* **2003**, *119*, 11099−11112.
(78) Cossi, M.; Scalmani, G.; Rega, N.; Barone, V. *J. Chem. Phys.* **2002**, *117*, 43−54.
(79) Krack, M.; Koster, A. M. *J. Chem. Phys.* **1998**, *108*, 3226−3234.
(80) Dreuw, A.; Head-Gordon, M. *Chem. Rev.* **2005**, *105*, 4009−4037.
(81) Glendening, E. D.; Badenhoop, J. K.; Reed, A. E.; Carpenter, J. E.; Bohmann, J. A.; Morales, C. M. *NBO 5.0*; Theoretical Chemistry Institute: University of Wisconsin: Madison, WI, 2001.

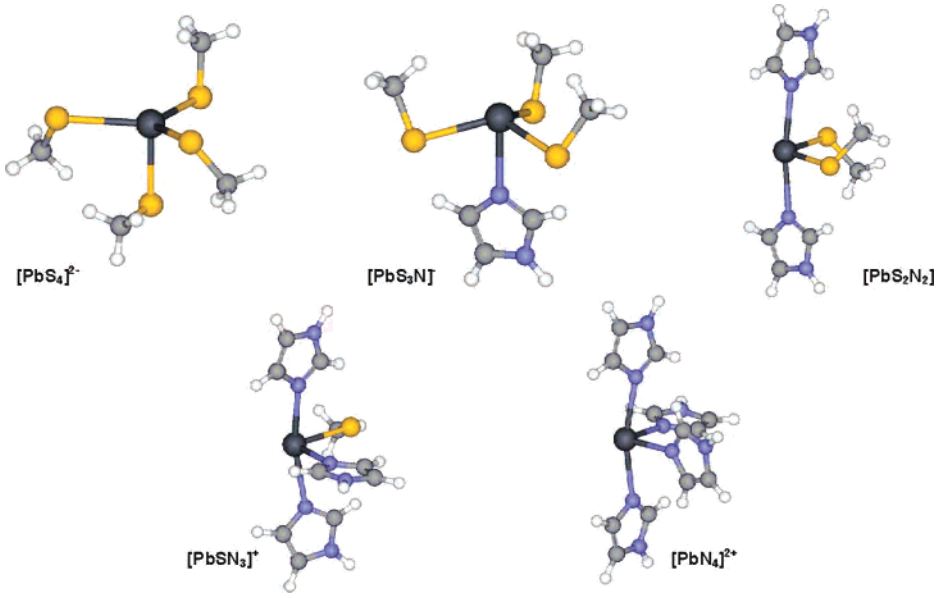

Figure 2. Molecular structures of tetracoordinated lead complexes in this study.

Table 1. Calculated Pb−ligand (Pb−S or Pb−N)[a] Bond Lengths (Å) and Selected Bond Angles (deg) for Modeled Lead(II) Complexes and Their Estimated Binding Energies (kcal/mol)

Molecular Complex	Local Sym. Group	R_1 (Å)	R_2 (Å)	R_3 (Å)	R_4 (Å)	α (deg)	β (deg)	γ (deg)	Binding Energy[b] (kcal/mol)
tri-coordination mode			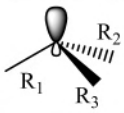			R_1-Pb-R_2	R_2-Pb-R_3		$E_B = E_c - E_i - \sum_l E_l$
$[PbS_3]^-$	C_s	2.710	2.700	2.700	-	97.7	93.9	-	-105.22
$[PbS_2N]$	C_1	2.610	2.626	***2.611***	-	91.5	88.2	-	-93.77
$[PbSN_2]^+$	C_1	2.582	***2.473***	***2.480***	-	89.0	88.5	-	-81.25
$[PbN_3]^{2+}$	C_3	***2.412***	***2.412***	***2.412***	-	90.3	90.3	-	-66.89
tetra-coordination mode A			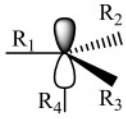			R_1-Pb-R_2	R_2-Pb-R_3	R_1-Pb-R_4	$E_B = E_c - E_i - \sum_l E_l$
$[PbS_4]^{2-}$	C_s	2.998	3.036	3.036	2.742	122.1	114.8	92.8	-97.87
$[PbS_3N]^-$	C_1	2.814	2.857	2.829	***2.605***	111.9	118.0	76.7	-94.35
tetra-coordination mode B			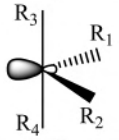			R_1-Pb-R_2	R_1-Pb-R_3	R_1-Pb-R_4	$E_B = E_c - E_i - \sum_l E_l$
$[PbS_2N_2]$	C_2	2.681	2.681	***2.747***	***2.747***	98.1	83.1	91.6	-94.45
$[PbSN_3]^+$	C_1	2.629	***2.486***	***2.654***	***2.681***	88.1	86.4	86.7	-85.23
$[PbN_4]^{2+}$	C_1	***2.429***	***2.455***	***2.600***	***2.631***	91.5	84.9	84.0	-73.59

[a] Pb−N bond distances are represented by bold italic font. [b] Based on computed DFT energies including PCM solvation and zero-point energy correction: E_c, energy of the complex; E_i, energy of a free lead ion; E_l, energy of a coordinated ligand.

B for $[PbS_2N_2]$, $[PbSN_3]^+$, and $[PbN_4]^{2+}$ complexes that are characterized by two weakly bound axial ligands and two strongly bound equatorial ligands. Both coordination modes are predicted by the VSEPR model but differ by the position of the lone-pair orbital. In mode A, the pair occupies the axial position, and in mode B, it occupies one of the three equivalent equatorial positions. Considering the VSEPR lone-pair−bond-pair repulsion factor, the structures with the coordination mode B are expected to be more stable. In structures of mode B, the lone pair is at an angle of 90° to two of the bonding pairs, but in structures of mode A, it is at an angle of 90° to three of the bond pairs. Therefore, the electrostatic repulsion should be less in the former than in the latter configuration, and the former is, in fact, the most commonly observed structure for AX_4E coordination. This type of coordination is classically viewed as a result of the $sp^2 + pd = sp^3d$ hybridization of valence orbitals of the central atom.

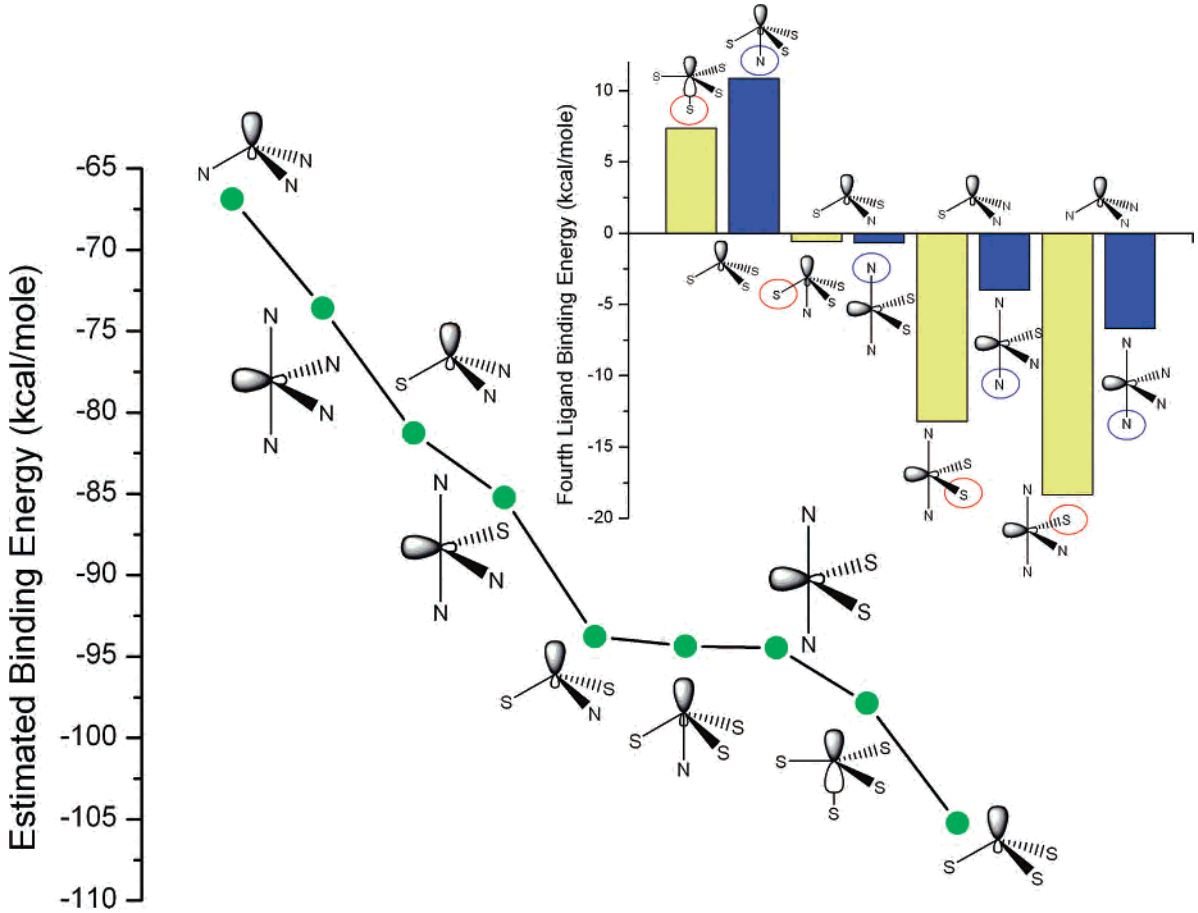

Figure 3. Estimated PCM DFT binding energies for computed lead complexes, computed according to the formula $E_B = E_c - E_i - \Sigma_l E_l$. Inset: Estimated formation energies of tetracoordinated lead complexes from corresponding tricoordinated lead complexes computed according to the formula $E_F = E_{B,tetra} - E_{B,tri}$.

The existence of both coordination modes, predicted by the electronic structure calculation for tetracoordinated lead complexes, and a larger stabilization of mode A complexes (see below) pinpoint a fact that the classical interpretation of the disposition of ligands around lead caused by the stereochemically active lone pair might be too simplistic or simply incorrect. Indeed, other quantum mechanical studies have come to similar conclusions. For instance, theoretical investigation of the origin of the asymmetric distortion observed in α-PbO crystals[74] has given an alternative interpretation of crystal asymmetry, suggesting that it could be caused by partial occupation of antibonding molecular orbitals of lead, giving rise to antibonding interactions and asymmetry in lead structures. Similarly, the natural orbital analysis performed on tetracoordinated lead structures reported here and by Shimoni-Livny et al.[53] do not show any significant contribution of lead 6d orbitals, which would advance the formation of the sp^3d hybrids in accord with the classical interpretation.

Closer examination of the structural parameters of computed complexes and their detailed orbital analyses (see below) has advanced and supported an alternative view for the tri- and tetracoordinated structures of lead that are investigated here. Observed changes in the structure of lead complexes might be viewed as a balanced combination of two factors: (A) the stabilization of the stereochemically active lone-pair orbital by ligands and (B) the extension of the s−p orbital mixing. Both factors are strongly modulated by the partial occupation of virtual 6p orbitals of lead that are differently influenced by the ligand's sulfur and nitrogen donor atoms.

Unlike nitrogen, sulfur is a strong donor of 3p electrons to lead 6p orbitals. These orbitals overlap strongly when thiolates are coordinated to the metal. Donation of the electron pair from the sulfur 3p orbital forms a strong Pb−S σ bond that correlates with a decrease of the bond distance. However, while the Pb−S bond is strengthened, the stereochemically active Pb($6s^2$) orbital is destabilized, due to its increased overlap with the occupied 3p orbitals of sulfur. Therefore, to maximize the bonding overlap between 3p sulfur and 6p lead orbitals and at the same time minimize the antibonding overlap between 3p sulfur and $6s^2$ lead orbitals, the mixing of lead's s−p orbitals is minimized. This keeps the s-character electrons closer to the center of the lead ion.

Consequently, tetracoordinated structures of mode A strongly bind only one axial ligand, employing a "pure" $6p_z$ orbital and three weakly bound equatorial ligands with sp^2 hybrids formed to stabilize the $6s^2$ orbital and accommodate the fourth ligand ($p_z + sp^2$). In mode B, two equatorial ligands are strongly bound, employing pure $6p_x$, $6p_y$ orbitals,

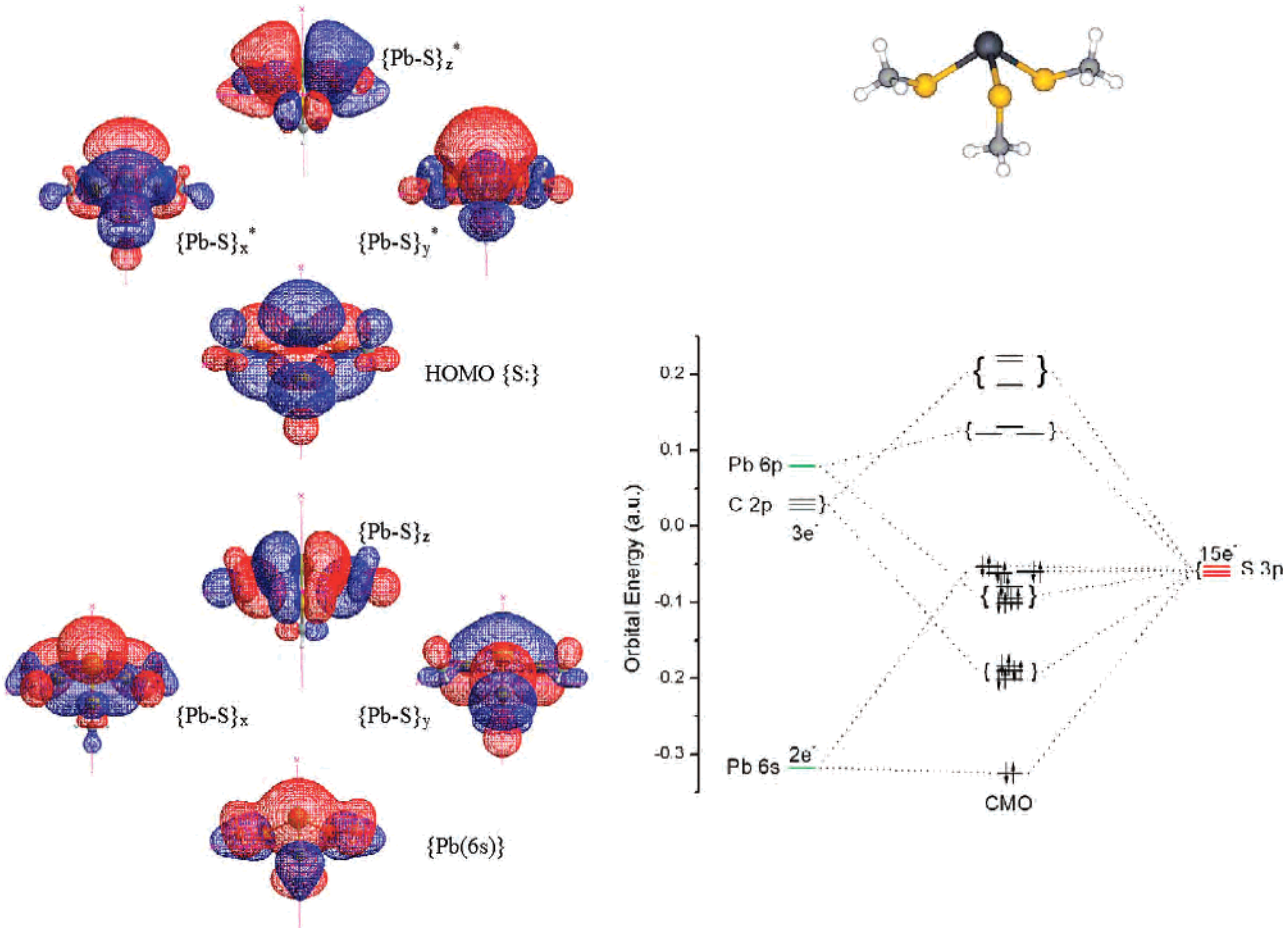

Figure 4. Illustration of wavefunction (iso value = 0.01e) and orbital energy diagram of selected molecular orbitals for the $[PbS_3]^-$ complex.

and two weak axial ligands are bound, employing sp hybrids (p_x, p_y + sp).

In the tricoordinated structures, the structural effects of partial occupation of Pb(6p) orbitals and minimization of the s−p orbital mixing to stabilize the Pb($6s^2$) orbital is less noticeable due to the reduced number of ligands. However, there is still a strong structural and electronic indication that formed metal−ligand bonds employ pure $6p_x$, $6p_y$, $6p_z$ metal orbitals and stabilize a pure $6s^2$ orbital (p_x, p_y, p_z + s).

Structural Parameters. Selected geometric parameters, bond distances, and angles of computed complexes are collected in Table 1. The average Pb−S distance in the computed structures decreases as the number of coordinated thiolates reduces in the order $[PbS_4]^{2-}$, $[PbS_3N]^-$, $[PbS_3]^-$, $[PbS_2N_2]$, $[PbS_2N]$, $[PbSN_3]^+$, and $[PbSN_2]^+$. A typical Pb−S bond distance is found in a range from about 2.6 to around 2.7 Å, which is in good agreement with a typical lead−thiolate bond found in crystallography and X-ray absorption spectroscopy. For example, the average Pb−S distance at around 2.64 Å has been found for a trigonal-pyramidal coordination of lead in the $[(C_6H_5)_4As][Pb(SC_5H_6)]$ crystal structure.[33] Similarly, the X-ray determination of the $\{[Tm^{Ph}]$-$Pb\}^+$ structure[41] (Tm^{Ph}−tris(2-mercapto-1-phenylimidazolyl)-hydroborate ligand), which is a model compound for the inactivation of the ALAD enzyme by lead poisoning, has reported a Pb−S distance at around 2.69 Å. This distance range was also confirmed by recent X-ray absorption spectroscopy on lead(II) bound to structural model zinc-binding peptides[18] where the Pb−S bond was found at around 2.64 Å. Deviations from this typical range are predicted only for weakly bound equatorial ligands in tetracoordinated complexes of mode B with Pb−S computed distances ranging from about 2.8 to about 3.0 Å. These longer Pb−S bonds have also been observed experimentally in crystals with a higher number of sulfur atoms in lead's coordination sphere. For example, X-ray structure determination of lead ethane-1,2-dithiol crystals[34] identifies lead coordinates with as many as six sulfur atoms; two of them at a typical distance of ca. 2.65 Å, the other two at ca. 3.04 Å, and the remaining two at a very long distance of ca. 3.48 Å.

A typical Pb−N distance with nitrogen from an imidazole ligand is predicted to be shorter than a typical Pb−S distance and computed to fall into the 2.4−2.6 Å range. This is expected, since the radius of the nitrogen donor atom is about 2.5 times smaller than the radius of the sulfur ion. The only deviation from this range is found for weak axial ligands in tetracoordination complexes of mode A, for which the range is around 2.65−2.75 Å. These bond lengths also agree well with the X-ray structure characterization of model compounds such as lead cysteamine complexes[59] and a recently synthesized model compound, N_2S(alkylthiolate)lead.[45] These reports have identified the Pb−N bond distances at 2.41 and 2.59 Å for cysteamine crystals[59] and at 2.49 and 2.53 Å for {2-methyl-1[methyl(2-pyridin-2-ylethyl)amino]propane-2-

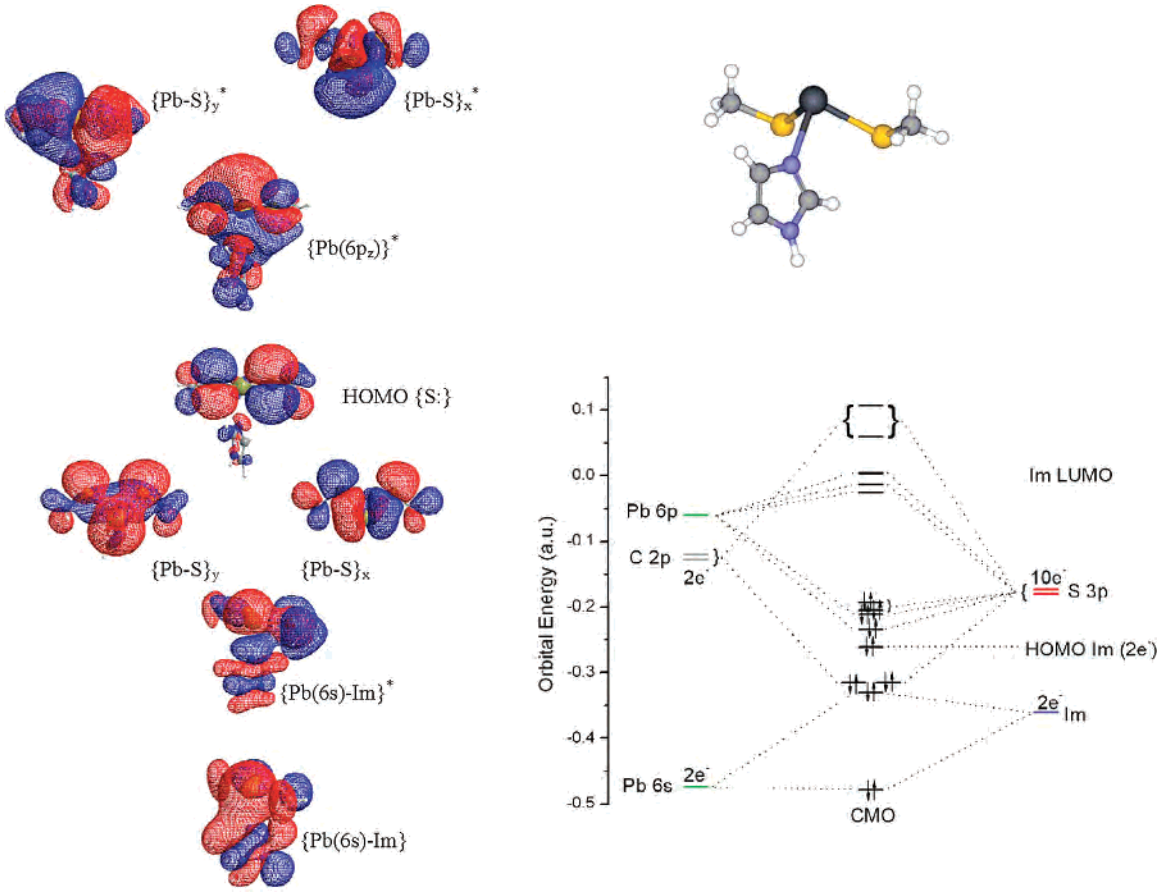

Figure 5. Illustration of wavefunction (iso value = 0.01e) and orbital energy diagram of selected molecular orbitals for the $[PbS_2N]$ complex.

thiolatolead perchlorate} ([PATH-Pb][ClO_4]) crystals.[45] All these observations are within a range predicted for a typical Pb−N distance.

Computed bond angles for all tricoordinated complexes are all closer to 90° rather than to 109°28′, as would be expected for a basic AX_3E tetrahedral structure.[51] These results are consistent with X-ray data[33,34,45,59] and might suggest that the extent of orbital mixing between lone pair ($6s^2$) and 6p orbitals in tricoordinated lead is minimal and that the metal employs pure 6p orbitals to form bonds with the ligands rather than the hybridized sp^3 orbitals. Similarly, the expected angles between equatorial ligands for tetracoordinated structures are expected to be close to 120° (assuming sp^3d hydridization of the metal). However, the only structures with the equatorial ligand angles close to 120° are within the mode A coordination, while computed angles for structures within the mode B coordination are all closer to 90°. Furthermore, the natural orbital analysis for the tetracoordinated structures does not indicate any mixing of lead's 6d orbitals that would support formation of the sp^3d hybrids.

Stabilization Energies. The stabilization or binding energies of the computed complexes have been estimated in an aqueous solution from the computed PCM DFT energies with inclusion of the zero-point energy correction for each computed complex and its appropriate number of fragments: free thiolates, free imidazoles, and a lead ion. The binding energies computed as a difference in the energy of the complex (E_c) and the energies of a free lead ion (E_i) and free ligands (E_l) are listed in Table 1 and shown in the comparison plot in Figure 3. This simple approximation of stabilization of computed complexes indicates that a tricoordinated $[PbS_3]^-$ complex is the most stable structure while the $[PbN_3]^{2+}$ complex is the least stable structure, which is in good agreement with experiments that reveal a strong preference of lead to form thiolate-rich structural domains in poisoned proteins.[15−18] Besides the $[PbS_3]^-$ complex, four other structures of tetracoordinated $[PbS_4]^{2-}$, $[PbS_3N]^-$, and $[PbS_2N_2]$ complexes and tricoordinated $[PbS_2N]$, all with at least two coordinated thiols, show relatively strong computed binding energies of about 94 kcal/mol or higher.

The estimated energy cost to accept the fourth ligand (thiolate or imidazole) to various tricoordinated complexes is shown in the inset of Figure 3. The graph illustrates that to accept a thiolate as the fourth ligand by a tricoordinated lead complex is always energetically easier than to accept an imidazole ligand. This relatively simple estimate of energies is consistent with recent reports that the tricoordination of lead in poisoned sulfur-rich proteins is preferable[18] but also points out that some tetracoordinated structures might still be considered as plausible lead domains.

Molecular Orbital Analysis. A set of five lead complexes, $[PbS_3]^-$, $[PbS_3N]^-$, $[PbS_2N_2]$, $[PbS_2N]$, and $[PbS_4]^{2-}$, has been computationally evaluated to be most stable. The set represents a full spectrum of coordination modes that are described above. Their electronic structure has been explored

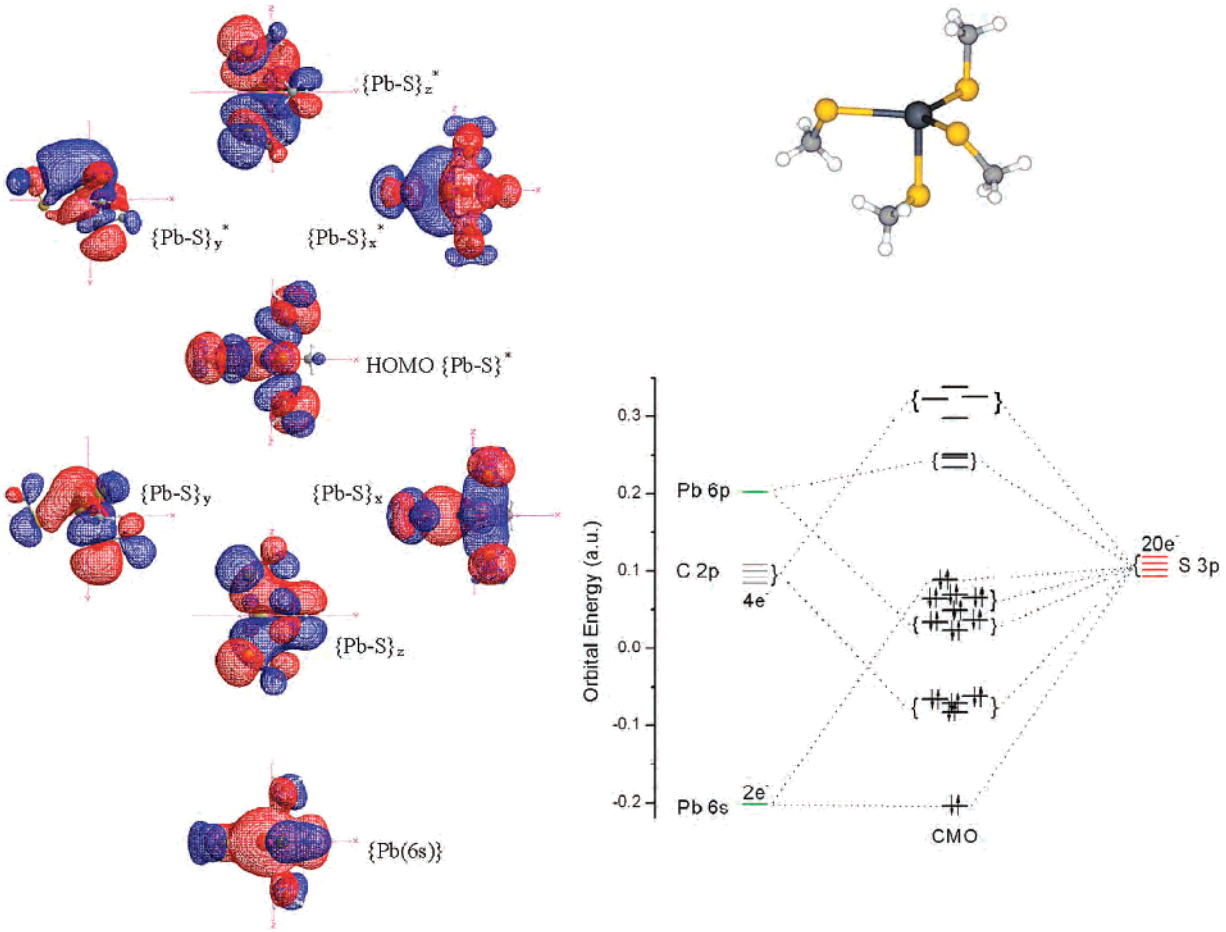

Figure 6. Illustration of wavefunction (iso value = 0.01e) and orbital energy diagram of selected molecular orbitals for the $[PbS_4]^{2-}$ complex.

in detail by employing the canonical molecular orbital analysis. The essential results are illustrated for tricoordinated structures: $[PbS_3]^-$ in Figure 4 and $[PbS_2N]$ in Figure 5; tetracoordinated structures of mode A $[PbS_4]^{2-}$ in Figure 6 and $[PbS_3N]^-$ in Figure 7. Finally, the tetracoordinated structure of mode B is represented by $[PbS_2N_2]$ in Figure 8.

For clarity of presentation, only selected molecular orbitals are shown for each structure along with the simplified molecular orbital diagrams. Each diagram highlights the stereochemically active orbital of lead Pb(6s), the molecular orbitals of Pb−S and C−S bonds, and in the complexes with the imidazole ligand present, the lead−imidazole σ orbitals, the highest-occupied (HOMO) and the lowest-unoccupied (LUMO) molecular orbitals of imidazole ligands. Pictures of selected molecular orbitals are shown in order of increasing energy: (a) Pb(6s) orbital or its binding and antibonding combinations with imidazole σ orbital, (b) Pb−S binding orbitals, (c) the HOMO orbital of a complex, (d) and finally, the LUMO, LUMO + 1, and LUMO + 2 of a complex. All shown orbitals have been chosen for their importance in interpretation of the electronic excitation spectra in the UV region (discussed below).

The natural bond analysis of the Pb−S orbitals in all complexes has revealed that the bonding orbitals have as much as about 80% contribution from the 3p orbital of sulfur atoms and only around 20% contribution from the 6p orbital of lead, while the antibonding Pb−S orbitals are the reverse, as here about 20% of the contribution is coming from the 3p orbital of sulfur atoms and about 80% of the contribution is coming from the 6p orbital of lead. This can be easily noticed in the orbital shapes of the LUMO, LUMO + 1, and LUMO + 2 of the complexes, which retain the basic shape and orientations of the $6p_x$, $6p_y$, and $6p_z$ atomic orbitals of lead. Hence, the electron density of the Pb−S bonding orbitals is mostly localized on sulfur atoms while the electron density of the Pb−S antibonding orbitals is largely localized on a lead ion.

Consequently, it is worth pointing out that the remaining lone-pair orbitals of sulfur atoms, which for most structures are the HOMO orbitals, are energetically quite close to the bonding Pb−S orbitals and, therefore, are likely to participate in CT electronic transitions. The Pb−S orbital energies are usually slightly lower than the orbital energies of sulfur's lone-pair orbitals. However, in complexes with mode A coordination (see Figures 6 and 7), one of the Pb−S orbitals gets strongly destabilized due to augmented ligand interaction with the $Pb(6s^2)$ orbital, and its orbital energy is increased to take the HOMO status.

Unlike sulfur, nitrogen donor atoms do not overlap or interact with 6p orbitals of lead due to the much lower orbital energy of nitrogen 2p orbitals. This is clearly demonstrated in the molecular orbital analysis when the thiolates are consecutively replaced by imidazole ligands. In complexes with an increased number of imidazole ligands, the 6p

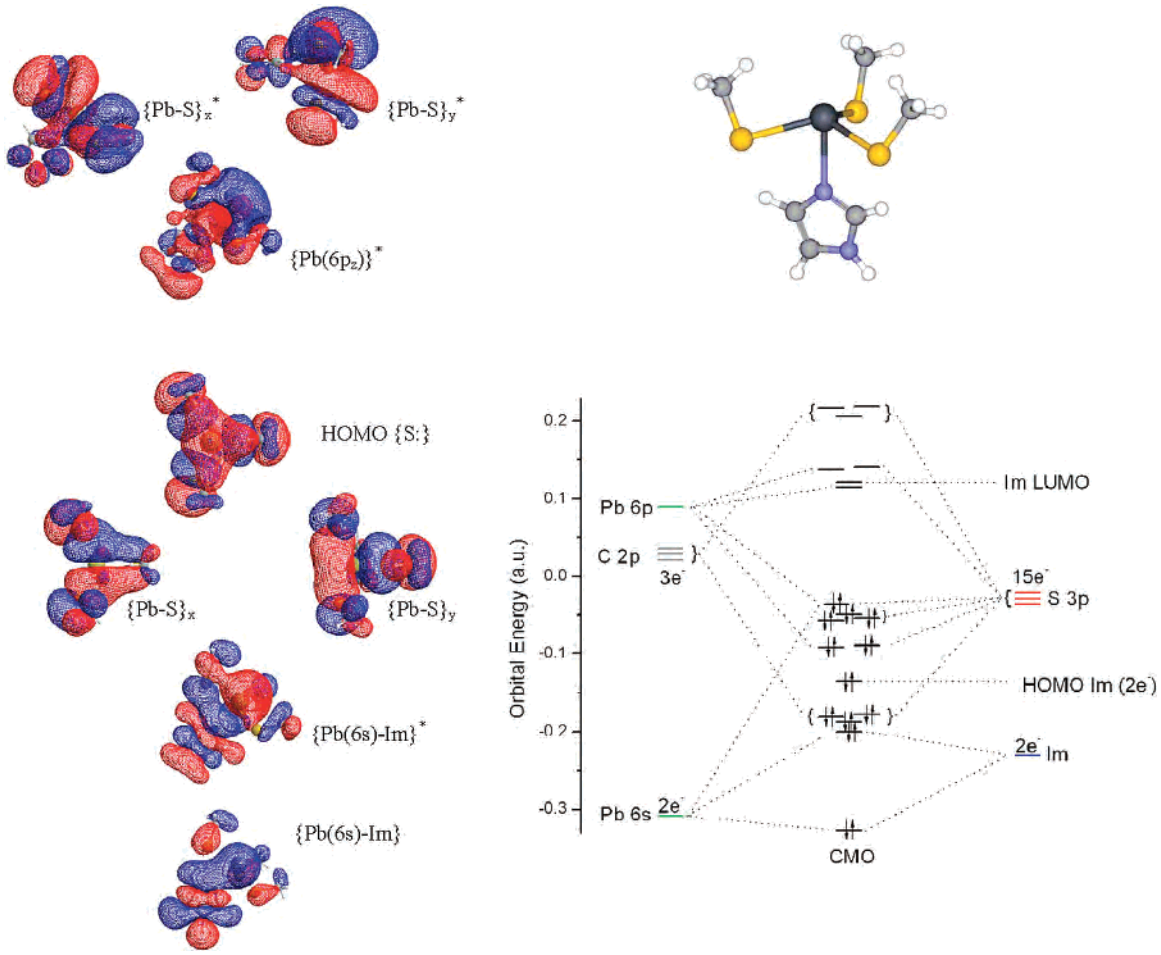

Figure 7. Illustration of wavefunction (iso value = 0.01e) and orbital energy diagram of selected molecular orbitals for the $[PbS_3N]^-$ complex.

orbitals of lead do not form the molecular orbitals but stay largely unperturbed as virtual lone-pair orbitals. The number of released 6p orbitals depends on the corresponding number of coordinated thiolates. For example, two thiolates employ only two 6p orbitals to form two PbS bonds, and one 6p orbital remains unperturbed, as can be seen in the molecular orbital diagram for $[PbS_2N]$ in Figure 5 and for $[PbS_2N_2]$ in Figure 8.

It should be noted that the LUMO orbital energy for imidazoles is energetically comparable to the antibonding Pb−S orbitals and/or the virtual Pb(6p) orbitals. Hence, it might be expected and indeed it is observed that the spectral intensity of the LMCT bands diminishes as the number of imidazole ligands increases, which is caused by the increased probability for an electron transition to the LUMO orbitals of the imidazole ligands instead of to the antibonding orbitals of lead.

Electronic Excitations and Spectral Analysis. A typical UV signal for lead-poisoned sulfur-rich proteins gives two characteristic well-resolved bands: a moderate intensity signal at around 330 nm and a strong signal at around 260 nm.[15,17,24,26,28] Both bands have been assigned to the electron transfer from S (3p) to Pb (6p) orbitals (LMCT bands) and have proved to be a significant spectroscopic probe for lead−protein bonding interaction. With the computations as a guide, we hope that these bands can be successfully employed to probe structural lead domains via resonance Raman spectroscopy, which has proven to be a very successful spectroscopic probe for metal structures and dynamics in proteins.

All simulated UV spectral lines computed by employing a 10 nm Lorentzian bandwidth to the TDDFT electronic excitations and their oscillator strengths are plotted in Figure 9. In addition to the tri- and tetracoordinated lead complexes, the spectral lines computed for the analogous set of zinc complexes ($[ZnS_4]^{2-}$, $[ZnS_3N]^-$, $[ZnS_2N_2]$, $[ZnSN_3]^+$, and $[ZnN_4]^{2+}$) are plotted on the same intensity scale. These spectra are shown for reference only to visualize the predicted intensity enhancement and other spectral changes expected when lead substitutes for typical zinc-finger domains.

The spectral composition and assignment of the excitations, with major contributions to the maximum bands for all computed complexes in the relevant UV region, are listed in Table 2. Two major trends are easily noticeable in the thiolate−lead CT band region shown in spectral comparison in Figure 9. First, the signal of the main band reaches maximum intensity for thiolate-saturated complexes, but its intensity quickly diminishes and blue-shifts when the number of imidazole ligands increases. The progress of these changes is rapid, and it is likely that for structural domains of lead coordinated to less than two cysteines, the LMCT band

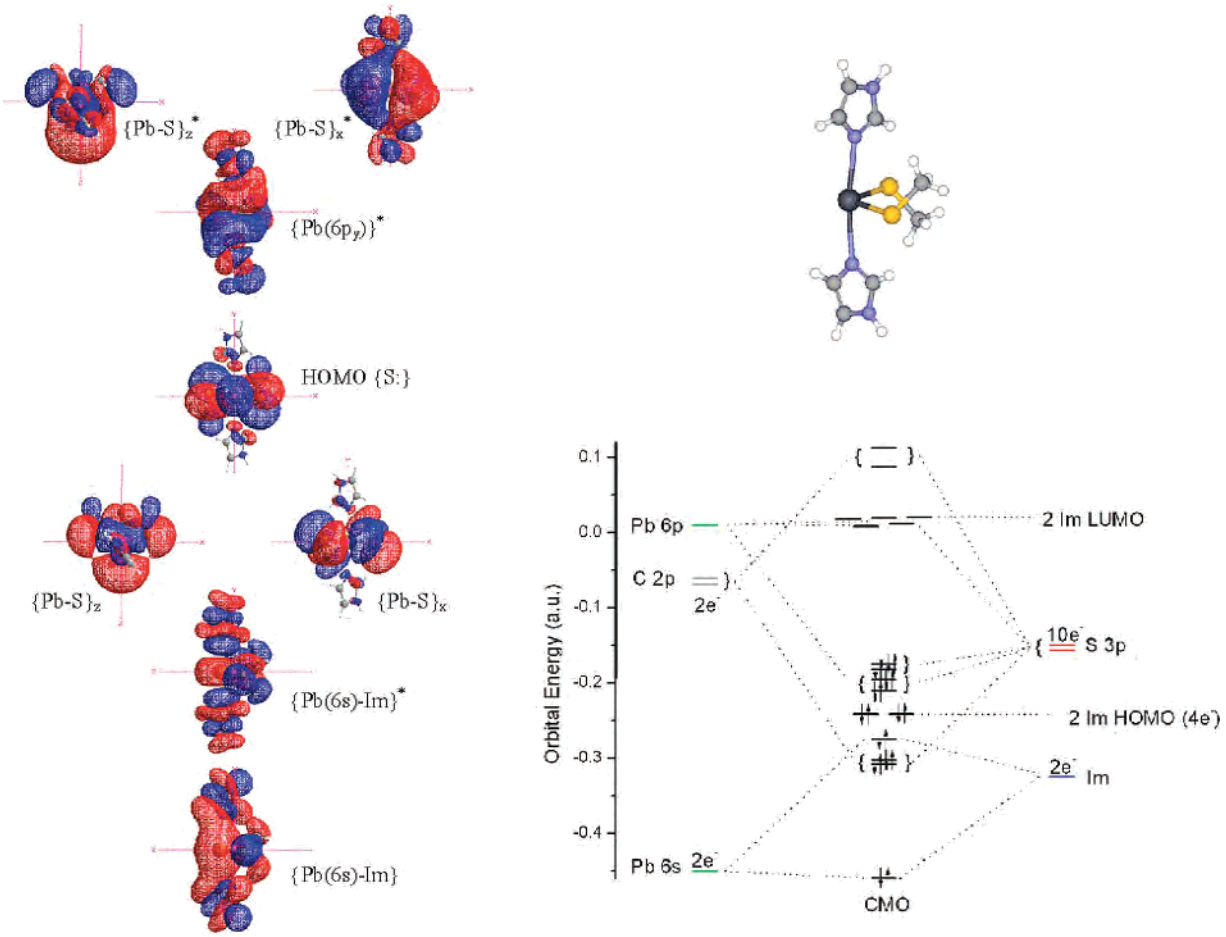

Figure 8. Illustration of wavefunction (iso value = 0.01e) and orbital energy diagram of selected molecular orbitals for the $[PbS_2N_2]$ complex.

becomes difficult to observe and not applicable or detectible in a protein environment.

Second, the maximum peak of the CT band linearly correlates with the average Pb−S distance. A maximum of the peak red-shifts as the average Pb−S bond length increases, as shown in the inset of Figure 9. This correlation, when properly scaled to experimental measurements, might be applicable for easy estimation of the average Pb−S bond length in lead's complexes of biological or environmental origin. For example, with the use of the linear relationship and a raw 45 nm empirical correction (see below) to refine the calculated data, a spectral band at about 258 nm observed for Pb(CP−CCCC) peptide corresponds to the average Pb−S bond length at around 2.72 Å, which compares favorably to the length of 2.64 Å from more-elaborate EXEFS spectral fits.[18]

Another important relationship between the molecular orbitals, structure, and electronic excitations might be expected when we consider the possible interplay of Pb−S molecular orbitals, lone-pair orbitals on sulfur atoms, and possibly on lead, as well as C−S bonding orbitals. It is well understood that the Pb−S bond is formed by the donation of a pair of electrons from the 3p orbital of a sulfur atom to the unoccupied 6p orbital of lead, but the remaining sulfur lone-pair orbital still might have a preference for a particular orientation to maximize the overlap with the remaining 6p orbitals of lead and/or interact with the Pb−S antibonding orbitals to stabilize the structure. This is apparent when the rotational conformation of the thiolates is examined, which consecutively modulates the extent of electron transition from sulfur lone-pair orbitals to lead in the CT band region. If guided via computational models, a possibly applicable consequence of this electronic relationship might show up when the environment imposes steric and electronic constraints on the structural lead domain and forces the ligands to orient to the environment-specific conformation. These environmental constraints might result in detectable differences in the UV spectral signal, which could be identified and assigned with help from computational studies. A simple example of such fine-tuned structure-spectra dependence might be anticipated by the predicted red-shift of the maximum band for $[PbS_3]^-$, $[PbS_3N]^-$, and $[PbS_4]^{2-}$ structures. The band shift correlates with an opening of the umbrella formed by three sulfur atoms coordinated to lead and thus with an increase of the s−p orbital mixing due to structural changes imposed by the fourth ligand.

The stability and function of metals in proteins have been developed through countless years of evolution, and in this respect, the domains of toxic metals should be viewed as a sudden stress on the protein that might lead to random responses and structures. As a result, the domains of poisoned proteins could be accidentally structured and driven by chemically less-specific paths than the structural domains formed by desirable, native metals. Therefore, a more realistic

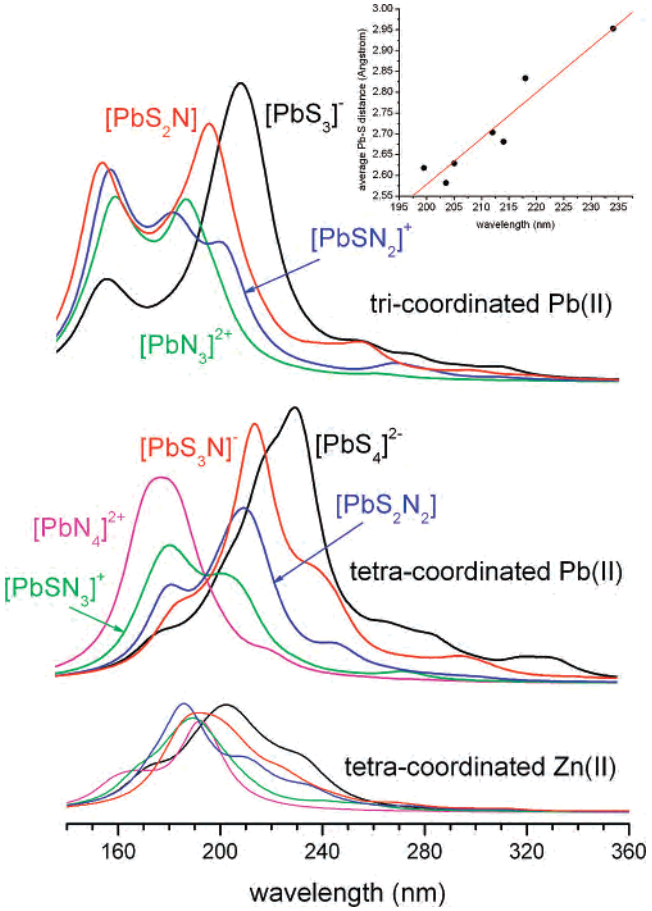

Figure 9. Comparison of computed TDDFT UV absorption spectra. Colors of unlabeled spectral lines of zinc complexes correspond to colors of spectral lines of appropriate tetracoordinated lead complexes. Inset: Correlation of the average Pb−S distance with a computed wavelength (λ_{max}) at maximum intensity of the CT band. Line equation: d_{Pb-S} (Å) = 0.3753 + 0.01102λ; R = 0.95579.

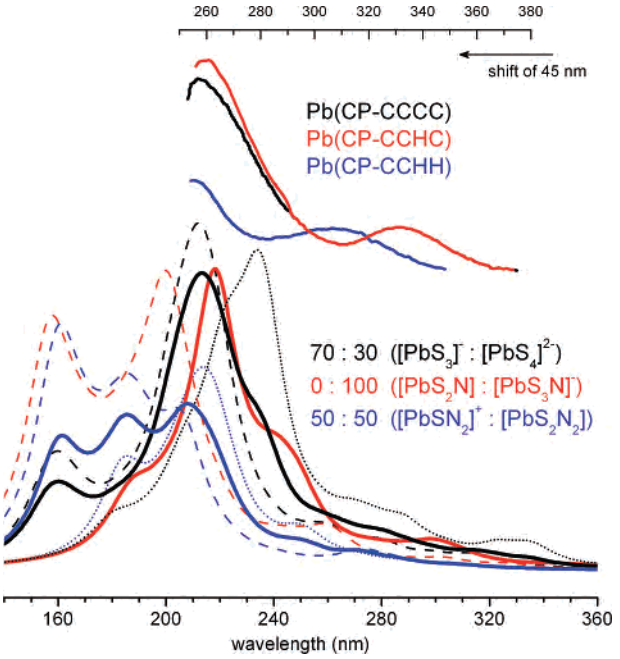

Figure 10. Experimental UV spectra for lead model peptides compared with computed UV spectra of model complexes: dashed lines, tricoordinated; dotted lines, tetracoordinated model complexes; solid bold lines, mixed, composed spectra with identified ratios of tri- and tetracoordinated model complexes.

view on structural lead domains in poisoned proteins should allow for partial randomness in formed domains, which might possibly explain some fine differences observed in the UV spectra for some proteins after exposure to lead, such as temperature dependence, in some severe cases leading to irreproducible spectra.[18] To illustrate these structural complexities, Figure 10 shows a direct comparison of the experimental UV signals of lead in model peptides[17] (Pb(CP-CCCC) with four cysteines, Pb(CP-CCHC) with three cystines and one hisitidine, and Pb(CP-CCHH) with two cystines and two histidines) with computed UV signals for tri- and tetracoordinated lead model complexes along with simulated signals of mixed assemblies of complexes with comparable ligand environment and estimated binding energies. The maximum bands of experimental spectra are found at around 260, 258, and 255 nm for Pb(CP-CCCC), Pb(CP-CCHC), and Pb(CP-CCHH), respectively. These compare to bands in computed spectra at 218, 213, and 209 nm for mixed assemblies $\{[PbS_3]^-/[PbS_4]^{2-}\}$, $\{[PbS_2N]/[PbS_3N]\}$, and $\{[PbSN_2]^+/[PbS_2N_2]\}$, respectively. After a simple refinement of spectra that red-shifts the computed spectra by 45 nm, the agreement is quite acceptable. In Figure 10, for a better visual comparison, the wavelengths of experimental vs computed spectra are adjusted and blue-shifted by 45 nm. This spectral shift is not unexpected and is commonly due to systematic errors associated with a given approximation in the electronic excitation calculations, usually caused by basis-set truncation and the necessary use of simplified structural models to mimic the particular protein environment.

The other, lower in energy LMCT bands with broader UV signals observed in experimental spectra at around 332 nm for both Pb(CP-CCCC) and Pb(CP-CCHC) peptides and at around 308 nm for the Pb(CP-CCHH) peptide are less resolved and distinct in computed spectra. This is caused by the relatively low oscillator strengths computed for these transitions. Nevertheless, some spectral features are still visible in computed spectra, and they could be correlated with features in the observed spectra, such as the weak signals at around 300 nm for $\{[PbS_3]^-/[PbS_4]^{2-}\}$, at around 280 nm for $\{[PbS_2N]/[PbS_3N]\}$, and at around 250 nm for $\{[PbSN_2]^+/[PbS_2N_2]\}$ composed spectra.

The ratios of complexes in the composed spectra have been optimized based on a simple visual inspection to match the main spectral relations observed in the experiment. The proposed ratios should not be viewed as an attempt to make an accurate prediction of the relative composition of structural lead domains in these peptides, solely based on good agreement with experimental spectra, but rather viewed as an example which demonstrates the possibility of the structural diversity of lead domains in poisoned proteins. This issue of the plausible diversity of lead structures identifies structural complexity, which is necessary to investigate to advance our understanding of the mechanisms of lead toxicity, and calls for more structural and dynamic probes of lead domain formation, such as resonance Raman spectroscopy guided by model calculations.

Table 2. Selected TDDFT Excited States and Electronic Transitions for Lead Model Complexes

molecular complex	local sym group	λ_{max}[a] (nm)	peak composition at λ_{max}[a,c]	assignment[b]
			tricoordination mode	
$[PbS_3]^-$	C_s	212.0	24% of (λ_{17} = 217.6, f = 0.4070) A′	44% (PbS → PbS*) + 21% (S: → CS*)
			32% of (λ_{19} = 211.7, f = 0.4202) A″	42% (PbS → PbS*) + 40% (S: → CS*)
			19% of (λ_{20} = 209.3, f = 0.2647) A″	68% (S: → CS*) + 18% (PbS → PbS*)
			13% of (λ_{21} = 202.4, f = 0.3379) A′	69% (PbS → PbS*) + 3% (S: → CS*)
$[PbS_2N]$	C_1	199.5	47% of (λ_{22} = 200.3, f = 0.5299)	42% (PbS → PbS*) + 13% (S: → Im*) + 10% (PbS → Im*)
			13% of (λ_{23} = 198.9, f = 0.1422)	53% (S: → Im*) + 18% (S: → CS*) + 8% (PbS → PbS*)
			10% of (λ_{24} = 198.4, f = 0.1071)	36% (S: → CS*) + 24% (PbS → CS*) + 20% (S: → Im*)
$[PbSN_2]^+$	C_1	203.5	29% of (λ_{15} = 207.2, f = 0.2061)	46% (Im → PbS*) + 26% (PbS → PbS*) + 5% (PbS → Im*)
			25% of (λ_{17} = 205.1, f = 0.1557)	58% (Im → PbS*) + 18% (PbS → PbS*) + 6% (S: → Im*)
$[PbN_3]^{2+}$	C_3	190.5	38% of ($\lambda_{22,23}$ = 190.9, f = 0.1555) E	48% (Im → Pb(6p)*) +34% (Im → Im*)
			20% of (λ_{24} = 190.6, f = 0.1563) A	71% (Im → Im*) + 6% (Im → Pb(6p)*)
			tetracoordination mode A	
$[PbS_4]^{2-}$	C_s	234	33% of (λ_{21} = 236.2, f = 0.4126) A″	80% (PbS → PbS*) + 3% (S: → PbS*)
			31% of (λ_{22} = 234.5, f = 0.3720) A′	66% (PbS → PbS*) + 18% (S: → PbS*)
$[PbS_3N]^-$	C_1	218	38% of (λ_{30} = 218.8, f = 0.4347)	77% (PbS → PbS*) + 2% (S: → PbS*)
			48% of (λ_{31} = 217.7, f = 0.5466)	74% (PbS → PbS*) + 3% (S: → PbS*)
			tetracoordination mode B	
$[PbS_2N_2]$	C_2	214	45% of (λ_{21} = 216.7, f = 0.3687) B	30% (PbS → PbS*) + 27% (PbS → Im*) + 18% (S: → Im*)
			27% of (λ_{24} = 208.9, f = 0.2638) A	35% (PbS → PbS*) + 33% (PbS → Im*) + 8% (S: → Pb(6p)*)
$[PbSN_3]^+$	C_1	205	17% of (λ_{17} = 213.4, f = 0.1383)	52% (CS → Pb(6p)*) + 17% (PbS → PbS*) + 8% (PbS → Pb(6p)*)
			14% of (λ_{18} = 209.2, f = 0.0758)	35% (CS → PbS*) + 34% (CS → Pb(6p)*) + 10% (PbS → PbS*)
			28% of (λ_{21}=204.4, f = 0.1351)	41% (S: → Im*) + 13% (PbS → PbS*) + 10% (PbS → Im*)
$[PbN_4]^{2+}$	C_1	181.5	13% of (λ_{40} = 177.7, f = 0.1273)	44% (Im → Im*) + 40% (Im → Pb(6p)*)

[a] The peak and its composition calculated based on the 10 nm Lorentzian half-bandwidth of the TDDFT nth electronic excitations at λ_n (nm) and their oscillator strength, f (atomic units). [b] Key: Asterisks stand for an antibonding character of a molecular orbital; PbS, molecular orbitals of Pb−S bonds; CS, molecular orbitals of C−S bonds; S:, a lone-pair orbital of sulfur; Im, molecular orbitals localized on imidazole; Pb(6p), a lone-pair orbital (6p character) of lead. [c] Electronic transitions λ_n with ≥ 10% contribution to the peak intensity at λ_{max}.

Although the presented structural models are quite simple when compared with the complexity of the enzymatic environment, our preliminary calculations on larger molecular models that increase the structural complexity have indicated that predicted spectral trends are well represented even by these simple models. In fact, when UV spectra for larger, more-realistic models were computed, the only major improvement was in the predicted absolute excitation values for the major UV bands. Nevertheless, we intend to continue with the theoretical investigation of lead's structures and coordination and spectroscopic properties, including resonance Raman spectroscopy, addressing the biological mechanisms of lead poisoning and complexity of environment.

Conclusion

We have presented a structural and spectroscopic theoretical investigation of simple models of mononuclear lead domains, which are possibly present in lead-poisoned proteins. We have demonstrated—in agreement with experimental data—that lead binds tightly, especially to cysteine-rich sites, and introduces new coordination preferences and structures that do not stabilize the proper form of structural zinc-binding domains. Electronic structure calculations, along with the molecular orbital analyses, have revealed that the classical interpretation of a major role of the stereochemically active lone-pair orbital in the observed structural diversity of lead complexes might be too simplistic. We have proposed that the optimal arrangement of lead's ligands is modulated by the extent of s−p orbital mixing and electronic stabilization of the lone-pair orbital, which is differently influenced by sulfur and nitrogen donor atoms.

Computed UV spectra have identified potentially applicable characteristic UV bands for lead complexes. The bands have been definitively assigned as the ligand-to-metal charge-transfer bands. Direct comparison of computed UV spectra with model lead peptides suggests a possibility of mixed structural domains coexisting in the poisoned protein environment. In light of the current study, more experimental probes, especially resonance Raman spectroscopy, and more elaborate theoretical investigations are anticipated and proposed to provide better understanding of the mechanisms of lead poisoning.

Acknowledgment. This work is supported by the National Institutes of Health Grant S06 GM076168.

Supporting Information Available: Computed Cartesian coordinates of all lead structures and computed DFT and PCM DFT energies. This material is available free of charge via the Internet at http:/pubs.acs.org.

IC700731D